

ARTICLE

OPEN



Printed elastic membranes for multimodal pacing and recording of human stem-cell-derived cardiomyocytes

Markos Athanasiadis^{1,6}, Dzmitry Afanasenkau^{1,6}, Wouter Derk^{2,6}, Christoph Tonner¹, Francesca Murganti², Volker Busskamp^{1,2,4}, Olaf Bergmann^{2,3} and Ivan R. Minev^{1,5}✉

Bioelectronic interfaces employing arrays of sensors and bioactuators are promising tools for the study, repair and engineering of cardiac tissues. They are typically constructed from rigid and brittle materials processed in a cleanroom environment. An outstanding technological challenge is the integration of soft materials enabling a closer match to the mechanical properties of biological cells and tissues. Here we present an algorithm for direct writing of elastic membranes with embedded electrodes, optical waveguides and microfluidics using a commercial 3D printing system and a palette of silicone elastomers. As proof of principle, we demonstrate interfacing of cardiomyocytes derived from human induced pluripotent stem cells (hiPSCs), which are engineered to express Channelrhodopsin-2. We demonstrate electrical recording of cardiomyocyte field potentials and their concomitant modulation by optical and pharmacological stimulation delivered via the membrane. Our work contributes a simple prototyping strategy with potential applications in organ-on-chip or implantable systems that are multi-modal and mechanically soft.

npj Flexible Electronics (2020)4:16; <https://doi.org/10.1038/s41528-020-0075-z>

INTRODUCTION

Recording and modulation in electrogenic tissues requires engineered systems, such as electrode arrays, microfluidics and optical fibres. It is recognized that such devices benefit from the introduction of materials that emulate the viscoelastic properties of biological systems. For example, in implanted electrode arrays, elastic substrates have improved long-term biointegration outcomes in tissues undergoing mechanical deformation^{1,2}. Similarly, cyborg organic electrodes engineered from conductive hydrogels may altogether eliminate the mechanical mismatch and enable control of the immune response^{3,4}. In vitro, elastic electrodes have made an impact for similar reasons. They have been used to monitor changes in stem-cell-derived monolayers under biomimetic cyclic strain or the electrical response of brain slices subjected to simulated mechanical trauma^{5,6}.

Elastic electrode arrays are most often used for stimulation or for recording of biopotentials. Their co-integration with other interfacing modalities is reported less frequently. Devices for sensing or delivery of biomolecules or for supplying light for optogenetics experiments are most often fabricated on non-elastic or rigid substrates^{7–9}. However, the development of multi-modal arrays that are also soft could be very attractive both for implanted and for in vitro applications. For example, as part of organ-on-chip systems they can be used to engage synergistic pathways for maturation and conditioning of stem-cell-derived microtissues. This can involve combinations of mechanical, optical, electrical and pharmacological pacing^{10,11}. Such systems should also provide real-time readout from integrated sensors^{5,12,13}. Progress in combining various interfacing modalities in closed-loop platforms is highlighted in recent reviews^{14,15}.

From a technological point of view, the fabrication of soft multi-modal arrays remains a challenge. Traditional microelectromechanical system fabrication processes are capable of engineering elasticity using intrinsically non-elastic materials such as silicon, metals and plastic foils at high integration densities limited only by the lithographic process^{16,17}. Integration of discrete elements such as light-emitting diodes (LEDs) with electrodes and sensors has also been demonstrated¹⁸. However, mastering these fabrication technologies is complicated, requires masks and alignment between separate layers and access to multiple tools in a cleanroom environment. Additive fabrication strategies developed for fabricating soft robots can be translated for the context of bioelectronic probes and skins^{19–23}. Among these, direct ink writing (a variation of three-dimensional (3D) printing) can facilitate patterning of multiple soft materials, such as silicones, silicone–microparticle composites or hydrogels. These inks can be engineered to have the physical properties necessary to carry electrical currents, light or liquid while preserving the elastic nature of devices^{23–25}. Organ-on-chip platforms produced in this way have already demonstrated electrical and mechanical readouts from cultured cardiac cells^{13,26,27}.

In this work, we develop an algorithm for direct writing of elastic membranes with embedded electrodes, waveguides and microfluidics (Fig. 1a, b). This is enabled by a palette of commercially available silicones processed via a multi-tool printer (Supplementary Fig. 1). We print prototype devices for liquid mixing and for organ-on-chip applications. These are used to demonstrate optical, pharmacological and electrical pacing and recording of human induced pluripotent stem cell (hiPSC)-derived cardiomyocytes (Fig. 1c). Despite a significant simplification of the fabrication process, our approach demonstrates an advancement

¹Biotechnology Center (BIOTEC), Center for Molecular and Cellular Bioengineering (CMCB), Technische Universität Dresden, 01307 Dresden, Germany. ²Center for Regenerative Therapies Dresden (CRTD), Center for Molecular and Cellular Bioengineering (CMCB), Technische Universität Dresden, 01307 Dresden, Germany. ³Department of Cell and Molecular Biology, Karolinska Institutet, SE-17177 Stockholm, Sweden. ⁴Present address: Universitätsklinikum Bonn, University of Bonn, Bonn, Germany. ⁵Present address: Department of Automatic Control and Systems Engineering, University of Sheffield, Mappin Street, Sheffield S1 3JD, UK. ⁶These authors contributed equally: Markos Athanasiadis, Dzmitry Afanasenkau, Wouter Derk. ✉email: i.minev@sheffield.ac.uk

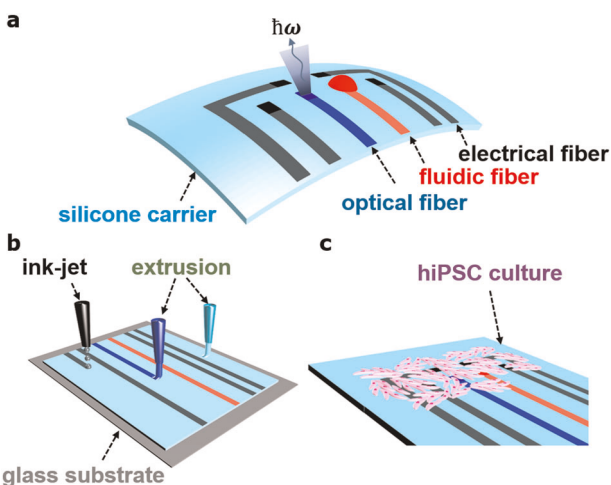


Fig. 1 Multimodal membranes for biointerfacing applications. **a** Concept for a sensor–actuator array with optical, electrical and microfluidic functionality. **b** Fabrication is handled by micro-extrusion and ink-jet-based direct writing. **c** Multimodal membranes can be integrated with cell monolayers for lab-on-chip applications.

of integration for multi-modal and mechanically compliant biointerfaces.

RESULTS

Functional fibre development

We start by printing freeform core–shell fibres where the core serves to guide light, electrical current or is left empty to carry fluid. Here all fibres are terminated with a contact site on one end and a connector on the other. For each fibre type, fabrication begins with structuring the shell from the shear thinning silicone elastomer SE1700 (Dow Corning), which can be extruded into self-supporting structures. First, a single straight line is printed directly on the glass substrate. A Π -shaped line is then printed around the straight line, creating a small opening at one end ($1200 \times 500 \mu\text{m}^2$), which will act as the cell culture contact site in the finished device (Fig. 2ai, Supplementary Fig. 2ai). Next, a second Π -shaped line is printed above the first one, forming a groove (Fig. 2aii, Supplementary Fig. 2aii). The core of waveguides is deposited directly within the groove using the optically transparent silicone elastomer OE6520 (Dow Corning). Since this silicone flows, it spreads to fill the cavity formed by the groove (Fig. 2aiii, Supplementary Fig. 2aiii). A top layer of SE1700 silicone seals the structure, serving as optical cladding (Fig. 2aiiv, Supplementary Fig. 2aiiv). Following thermal polymerization (120°C for 90 min), a step-index optical fibre is formed owing to the difference in the refractive index (RI) between the two silicones ($\text{RI}_{\text{OE6520}} = 1.54$ and $\text{RI}_{\text{SE1700}} = 1.44$). At this point, a custom cutting tool consisting of an angled razor blade is mounted on an empty printing nozzle. The tool is used to cut the end of the optical fibre at an angle of 45° followed by removal of the excess material (Fig. 2a(v, vi), Supplementary Fig. 2a(v, vi)). A layer of the white reflector silicone MS2002 (Dow Corning) is then deposited directly on the freshly cut surface. This structure serves as an angled mirror deflecting the path of light propagation by 90° (Fig. 2avii, Supplementary Fig. 2avii). The final printed optical fibres have dimensions of $600 \mu\text{m} \times 600 \mu\text{m} \times 5.5 \text{ cm}$ (width \times height \times length).

Fabrication of the electrically conductive fibres follows a similar procedure (Fig. 2b, Supplementary Fig. 2b). In this case, the functional core is formed by a conductive composite as described previously²⁴. Briefly, platinum microparticles ($\varnothing 0.2\text{--}1.8 \mu\text{m}$, ChemPur) are suspended in triethylene glycol monomethyl ether (TGME) by sonication with a tip sonicator, and the dispersion is

deposited inside SE1700 grooves by ink-jet. Subsequent evaporation of TGME leaves a compacted conductive mass of platinum microparticles. The core is sealed by deposition of polydimethylsiloxane (Sylgard 184), which fills the volume between platinum particles forming conductive composite. Since platinum particles are also deposited inside the opening left for the active site, a section of conductive material ($290 \times 250 \mu\text{m}^2$) remains exposed and later forms an electrical connection with cultured cells. The final printed electrical fibres have dimensions of $350 \mu\text{m} \times 350 \mu\text{m} \times 6 \text{ cm}$ (width \times height \times length).

For the fabrication of microfluidic fibres, we take advantage of the high yield stress of the SE1700 silicone, which allows reproducible printing of overhanging and high aspect ratio features. A bottom layer is first created (Fig. 2ci, Supplementary Fig. 2ci). Next, two additional Π -shaped lines are deposited, with a negative offset along the width of the structure. The resulting structure is pyramidal in shape and contains a hollow core (Fig. 2cii, Supplementary Fig. 2cii). The core has circular cross-section with diameter $D = 135 \mu\text{m}$. Here microchannel cores are formed directly during the printing process, which means that sacrificial inks and their subsequent flushing from the microchannels are not required²⁸. The printed fluidic fibres have dimensions of $350 \mu\text{m} \times 350 \mu\text{m} \times 5.2 \text{ cm}$ (width \times height \times length).

To embed the various fibres in a monolithic membrane, the area between them is filled with Sylgard 184. The final fabrication step is thermal polymerization (120°C for 45 min), after which the membrane is peeled from the glass substrate and inverted to expose the contact sites (Fig. 2d).

Functional fibre characterization

Next, in the context of their applications as electrodes, optrodes and chemotrodes for biointerfacing, we characterize the performance of printed structures. Using the cut-back method, attenuation in the optical fibres is measured to be $0.67 \pm 0.06 \text{ dB cm}^{-1}$ ($n = 5$) for blue light (470 nm) (Fig. 3a). This wavelength is chosen because it coincides with the action spectrum of the commonly used opsin Channelrhodopsin-2^{29,30}. Optical fibres are terminated with a contact site, which serves to couple light into cells cultured directly above. Deflection of the optical path is verified by immersing fibres in scattering media (milk) and observing light cones produced by the Tyndall effect (Fig. 3b). Optical losses due to light deflection by the contact site are measured to be approximately 0.32 dB. Active sites ($1000 \times 500 \mu\text{m}^2$) can supply maximum optical power density of 0.2 mW mm^{-2} when coupled to an external LED (Thorlabs M470F3, max. power 21.8 mW).

To characterise the electrical properties of electrodes formed by conductive fibres, we employ impedance spectroscopy (Fig. 3c). For electrodes with contact site dimensions of $290 \times 250 \mu\text{m}^2$ (Fig. 3d), we measure impedance modulus of $2.32 \pm 0.74 \text{ k}\Omega$ ($n = 5$) at a frequency of 1 kHz. These values are in good agreement with other platinum–silicone composite electrode coatings designed for recording and stimulation of extracellular biopotentials³¹. The frequency dependence of impedance is consistent with the Randles equivalent circuit model for electrodes immersed in electrolyte³². At low frequencies (below 1 kHz), the impedance of our electrodes is dominated by a capacitance arising from the electrochemical double layer at the electrode–electrolyte interface. At higher frequencies, the spectrum is dominated by the sum of the contact site spreading resistance and interconnect resistance, which are frequency independent and have phase angles close to 0° .

For the fluidic fibres, hydrostatic resistance experiments are conducted. Water is injected through sample fibres (length = 44 mm, lumen diameter = $135 \mu\text{m}$) at various pressures, and the resultant flow rates are measured (Fig. 3e). The fluidic fibres display microfluidic flow resistance of $4.93 \times 10^{-4} \pm 0.03 \times 10^{-4}$

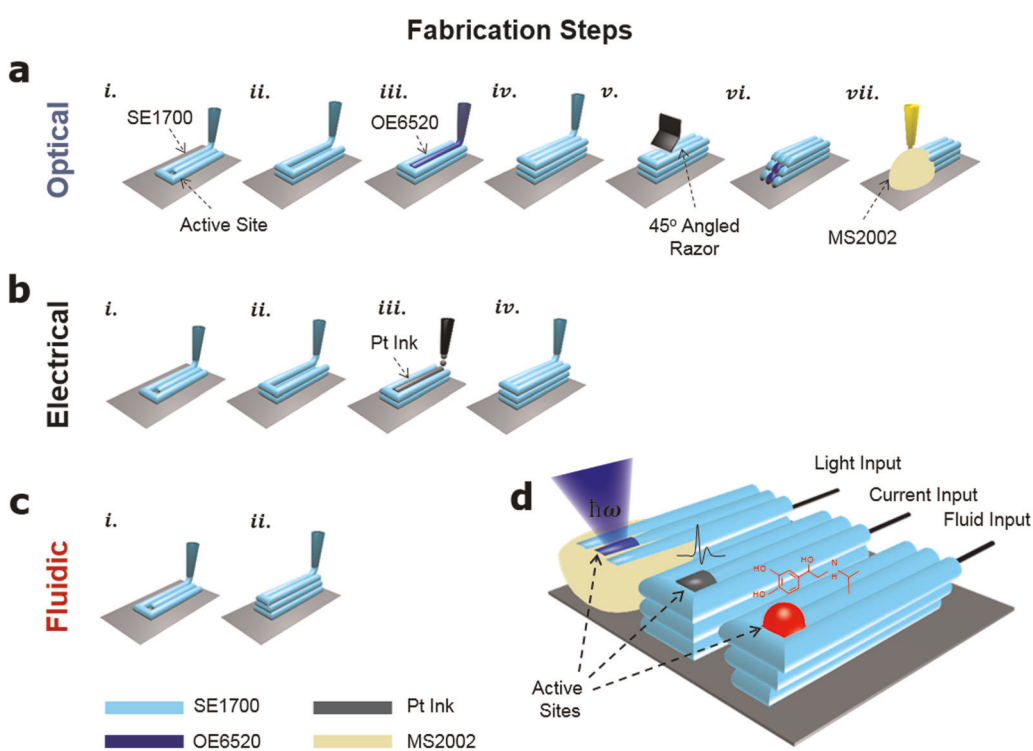


Fig. 2 Multi-material and multi-tool direct ink writing. Algorithm for the production of **a** optical, **b** electrical and **c** microfluidic fibres. The ink palette consists of a structural silicone (SE1700), high RI optical silicone (OE6520), optically reflective silicone (MS2002), all from Dow Corning, and a jettable dispersion of platinum microparticles. All printing tools are mounted on the 3DDiscovery bioprinter platform from RegenHU (Switzerland). **d** Following thermal polymerization, functional fibres are released from the substrate and inverted to expose active sites. The optical fibre is coupled with a conventional silica optical fibre (\varnothing 400 μm). The electrical fibre is coupled with a Teflon-coated steel wire. The fluidic fibre is coupled with a silicone tubing (\varnothing 200 μm).

$\text{Pa}\cdot\text{s m}^{-3}$, which is acquired by fitting of experimental data in a linear manner according to the Hagen–Poiseuille equation³³. Test fibres withstand liquid pressure of at least 1 bar without bursting. Moreover, printed fluidic fibres are obstruction free and support laminar flow even when printed in curved geometries, which is a good indication of homogeneity within the fibre (Fig. 3f(i, ii)). In addition, we demonstrate the ability to produce fluidic fibres, with bifurcation. Fork-shaped fluidic fibres could be used for the delivery of a fluid from several separate outlets (Fig. 3fiii). Finally, we demonstrate the ability to print T-Junction fluidic geometries, which could be employed for phase separation experiments. Specifically, we observe stable formation of water droplets in a mineral oil phase, following optimization of the flow rates in each channel (Fig. 3fiv, Supplementary Movie 1).

Generation of optogenetic hiPSC-derived cardiomyocytes

We used the fibroblast-derived hiPSC line CRTD5 and modified it to include a Cre-inducible Channelrhodopsin-2-EYFP (enhanced yellow fluorescent protein) expression cassette (Supplementary Fig. 3a)^{29,30}. We generated cardiomyocytes from the modified hiPSC line by modulating the Wnt signalling pathway (Supplementary Fig. 3b)³⁴. This yielded cardiomyocyte monolayers showing spontaneous contraction starting at 8 days in culture. Upon Cre administration, cells showed clear EYFP expression indicating successful optogenetic functionalisation (Supplementary Fig. 3c). All silicones used in the microphysiological platform (SE1700, OE6520, Sylgard 184, MS2002) supported hiPSC attachment and spreading (Supplementary Fig. 4). The platinum–silicone composite exhibited lower cell attachment; however, this was not observed to influence cell monolayer formation on integrated devices.

Integrated membranes

Individual printed fibres are embedded in a continuous membrane by casting a layer of Sylgard 184 silicone around them. Following thermal polymerization, the array is peeled from the substrate to expose the active sites. Once the fabrication method was finalized, we produced a batch of 10 devices that showed high yield and reproducibility. Among electrodes, 87% were functional (impedance $<100 \text{ k}\Omega$), similarly 80% of optrodes guided light (optical power $>0.1 \text{ mW mm}^{-2}$) and 90% of microfluidic channels had no leaks. Overall, 50% of the devices were fully functional. As illustrated in Fig. 4a, the multimodal membrane retains its elasticity and can be twisted and deformed without loss of functionality in its components. To contain cell culture medium, we additionally print a cylindrical chamber using SE1700 silicone (Fig. 4b). The finished device is connected to external stimulation and recording instrumentation via standard electrical wires, a silica optical fibre and microfluidic tubing (Supplementary Movie 2). This allows us to place the membrane inside a cell culture incubator and to control its operation from outside.

Following functionalisation with vitronectin, the membrane is seeded ($250 \text{ cells mm}^{-2}$) with optogenetically sensitized hiPSC-derived cardiomyocytes^{34,35}. The cells form a confluent monolayer covering the whole surface area of the integrated device. Within 3 days, cells display spontaneous periodic contractions (Supplementary Movie 3). Cultured monolayers express cardiomyocyte-associated markers such as cardiac troponin-T and connexin-43 in addition to Channelrhodopsin-2 (Fig. 4b, Supplementary Fig. 5). Electrical recordings confirm the presence of spontaneous activity. A typical field potential recorded has amplitude of $300 \mu\text{V}_{\text{pp}}$ and displays readily identifiable depolarization and repolarization peaks (Fig. 4c, Supplementary Fig. 6). We observed similar amplitudes and features in recordings obtained with commercially available microelectrode arrays (Supplementary Fig. 7).

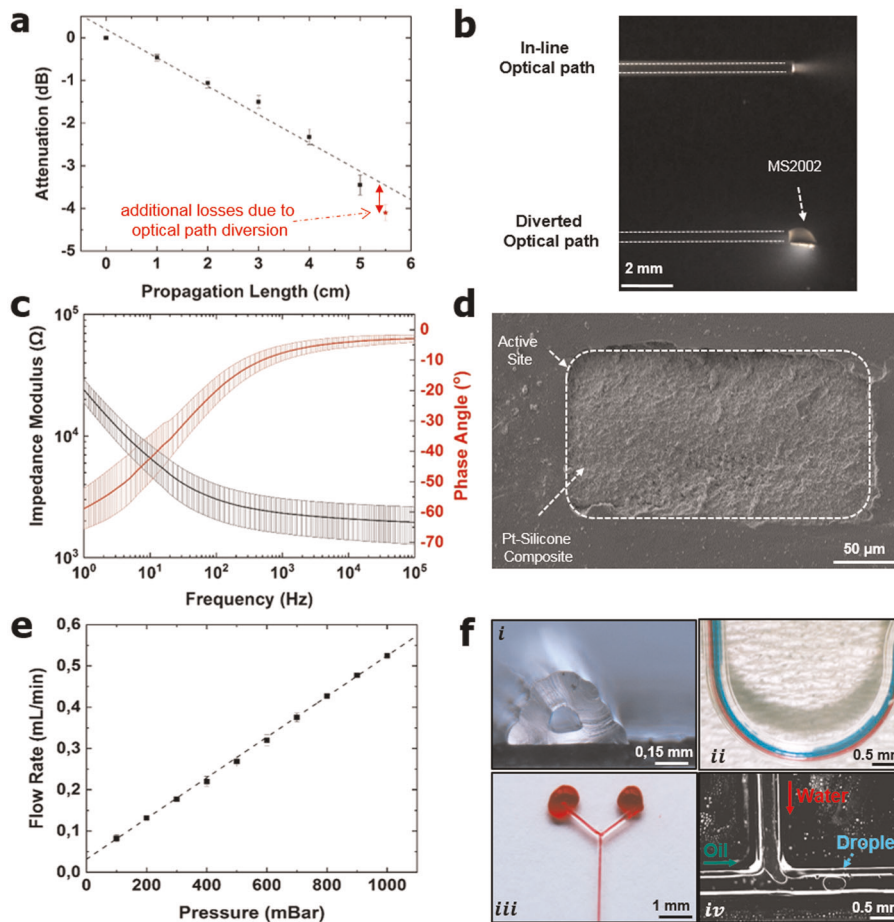


Fig. 3 Characterization of freeform functional fibres. **a** Optical attenuation of blue light (470 nm) along the length of optical fibres. The loss due to diverting light at the contact site is indicated in red ($n = 5$). **b** Optical photographs, demonstrating light emission from a straight terminated optical fibre and an optical fibre terminated with a contact site. Fibres are immersed in a solution of colloidal particles (milk). **c** Impedance spectra of printed electrodes immersed in phosphate-buffered saline (PBS) ($n = 5$). **d** Scanning electron micrograph (top view) of the contact site of a typical printed electrode. **e** Hydrostatic resistance of a printed microfluidic fibre. Fibre length and lumen diameter are 44 mm and 135 μ m, respectively ($n = 5$). **f** Micrographs of various fluidic fibre designs. Cross-section of a fluidic fibre illustrates the characteristic pyramidal shape of the structure (i). Freestanding fibres can be printed in curved shapes and support laminar flow inside the lumen (ii). Demonstration of a bifurcated microfluidic fibre eluting food dye from two outlets (iii) and a T-shaped junction for production of micro-droplets (iv).

In vivo, cardiomyocytes receive modulatory input not only from the endogenous electrical pacemaker of the heart but also from the endocrine system via hormones secreted by the adrenal gland³⁶. This adrenergic stimulation results in faster and stronger beating of the heart by shortening the duration of cardiomyocyte field potentials. To emulate these inputs via our microphysiological platform, we employ the microfluidic channel to deliver the non-selective β adrenoreceptor agonist isoproterenol directly in the culture chamber to a final concentration of 2 μ M. Within several seconds of the infusion, we observe a marked increase in the frequency of field potentials, from a spontaneous baseline of 0.25–0.75 Hz (Fig. 4d). The concomitant application of optical stimulation (0.2 mW mm^{-2}) via the optrode allows us to synchronize field potentials to a command frequency (Fig. 4d). Using this combined approach, we recorded field potentials occurring at rates up to 3 Hz where 1:1 correspondence to the optical trigger is maintained (Fig. 4d). Our approach allows us to access a wide range of pacing frequencies, which may be explained by shortening of the field potential by isoproterenol, which increases the likelihood of an incoming light pulse to trigger a further field potential³⁷. It is interesting to note that flow in the microfluidic channel may have contributed to increased excitability of the cardiomyocytes. This is because shear stresses are known to

activate mechanotransduction pathways resulting in recruitment of additional voltage-gated ion channels to the cell membrane³⁸.

DISCUSSION

We present a technological algorithm for printing membranes with integrated electrodes, optrodes and microfluidics for bioelectronic interfaces. Devices are realized from a selection of silicone elastomers, which ensures the mechanical compliance of the finished devices. Because we use inks with similar mechanical properties (silicone elastomers), we can integrate multi-modal functionality in a monolithic membrane with high yield and reproducibility (Fig. 3).

Devices with similar functionality can be assembled using other approaches. For example, a multi-modal array can be constructed by manually gluing optical fibres and cannulas to commercially available electrode arrays. However, such approach would be low throughput and may result in high batch variability. Alternatively, integration and miniaturization can be achieved via integrated circuit assembly of discrete elements, such as LEDs and microfluidics^{39,40}. However, this requires long development times and limits the number of design iterations that can be attempted by the end user at acceptable cost and accessibility. The

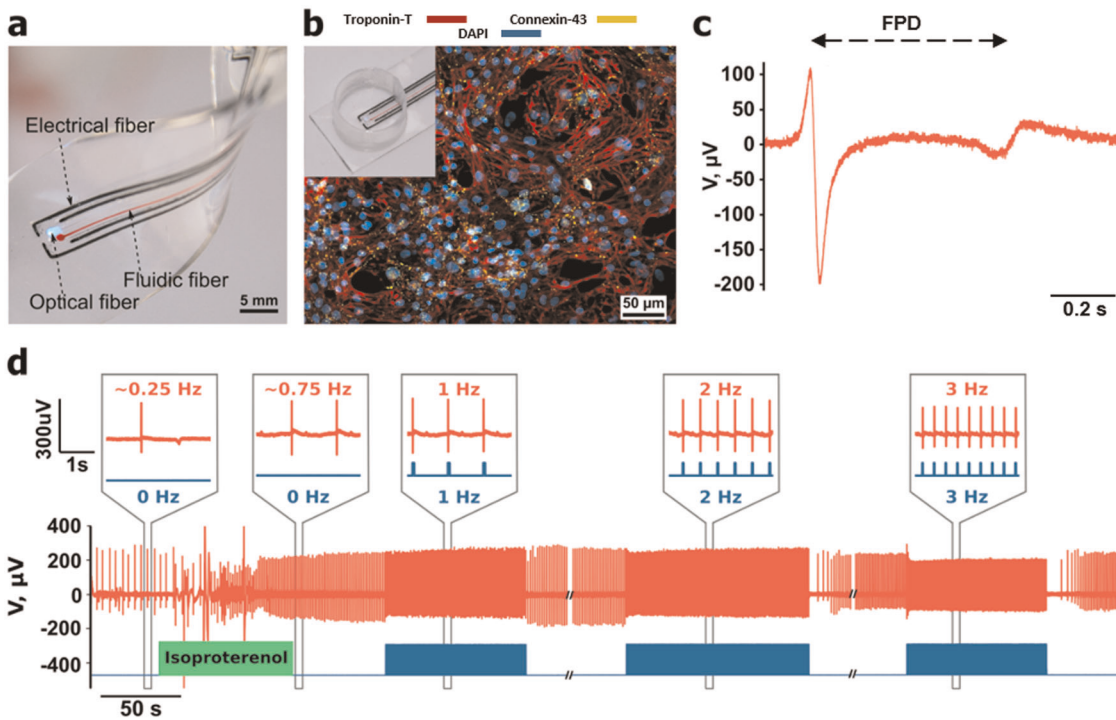


Fig. 4 Printed membrane for cardiomyocyte interfacing. **a** Integrated array of functional fibres where active sites form four electrodes, an optrode and a chemotrode. **b** hiPSC-derived cardiomyocytes cultured on the array express key cardiomyocyte markers troponin-T (red) and connexin-43 (yellow). Nuclei are labelled with DAPI stain (blue). Scale bar 50 μ m. Inset: membrane equipped with printed culture chamber. **c** Recording of spontaneous electrical activity (field potential) from hiPSC-CM. The waveform shows clearly visible depolarization due to Na^+ influx (first oscillation) and repolarization due to K^+ efflux (smaller second oscillation). The field potential duration (FPD) is 580 ms. The beat rate in this recording was approximately 0.15 Hz. **d** Bursts of optical pacing (blue) modulate the frequency of field potentials (red) generated in the cardiomyocyte monolayer. Insets show individual field potentials and their temporal relation to optical pulses. Infusion of isoproterenol increases baseline spontaneous activity. Additional pacing with optical bursts allows for further increase of field potential frequency (representative recording).

advantages of our printing methods are in its accessibility and simplicity. This is not at the cost of design flexibility as the layout of the membrane can be easily updated by changing the source CAD file.

Direct ink writing is a meso-scale technique that can routinely achieve sub-millimetre integration densities⁴¹. Similarly, in this work we write functional fibres spaced by approximately 0.5 mm and active sites with dimensions as small as $290 \times 200 \mu\text{m}^2$. The miniaturization available will not allow for interfacing individual cardiomyocytes but enables capture of field potentials representing activity in local patches of the cell monolayer. We show that recordings made with our membrane are comparable to those obtained with commercial but rigid multi-electrode arrays (MEAs; Multi Channel Systems, electrode diameter 30 μm , coated with a mixture of poly(3,4-ethylenedioxothiophene) and carbon nanotube) and enable observation of similar detail in the electrogram. Cells cultured on the membrane showed robust responses to pacing signals in the optical and pharmacological domain. This allowed us to make recordings in the absence of electrical stimulation artefacts. We did not yet demonstrate multi-modal recording/stimulation under tensile strains but acknowledge that emulating the dynamic mechanical environment of the heart in a dish could be important for advancing the field of cardiac tissue engineering. In the absence of external organizational cues, hiPSC formed a monolayer of randomly oriented cells. The continuation of this work may include the application of a combination of cyclic global strain and patterns of adhesive molecules to promote the organization of cells into a microtissue with biomimetic organization^{42–44}.

In this manuscript, we demonstrated the integration of sensing and actuation (stimulation) components using hybrid 3D printing.

The approach has the advantages of being widely available to the community while combining functional materials with elasticity similar to those of biological tissues. Because they present the opportunity to engage multiple pathways to maturation, soft and multimodal microphysiological platforms may enable qualitatively improved protocols for generating functional tissue *in vitro*.

METHODS

Ink preparation

Silicone elastomers, SE1700, OE6520 and MS2002 (Dow Corning), were prepared by mixing catalyst and base at a ratio of 1:10, 1:1 and 1:1, respectively, followed by degassing. For electrical fibres, conductive ink was fabricated by mixing platinum powder (particle diameter 0.2–1.8 μm , ChemPur, Germany) with TGME (Merck, KGaA), followed by tip sonication with Branson W-450 D sonifier (1/8" Tapered Microtip, 30% of power, 10 s/10 s pulse duration/delay). The platinum content in the suspension was around 15% by weight.

Printing

Printing was performed using the 3D Discovery bioprinter from RegenHU, Switzerland. Print layouts were developed in the BIOCAD software (RegenHU). The printed scaffolds for the functional fibres were developed with the SE1700 silicone, using a metal conical nozzle with a nominal inner diameter of 100 μm at the tip (Poly Dispersing Systems). The pneumatic pressure was set at 5 bar. The optical silicone OE6520 and the white reflector silicone MS2002 were deposited by the nozzle extrusion method using a nozzle of similar dimensions. The pneumatic pressures were set at 2 and 4 bar, respectively. The platinum suspension was deposited in the printed SE1700 scaffolds by ink-jet or by pipetting. The printed lines were then heated to 120 °C for 5 min to allow evaporation of TGME, leaving behind compacted dry platinum powder inside groove-shaped scaffolds.

In all cases, the substrate used for printing was glass treated with 2% sodium dodecyl sulfate (Merck KGaA) to form a debonding layer.

Optical fibres

Using the silicone SE1700, a straight line is printed directly on the substrate. Next, a Π -shaped line is printed around the straight line, creating a small opening at one end ($1200 \times 500 \mu\text{m}^2$), which will act as the cell culture contact site in the finished fibre. A second Π -shaped line is then printed above the first one, forming a groove. One end of a cleaved silica optical fibre ($\varnothing 400 \mu\text{m}$, Thorlabs) is placed inside the recently printed groove. The core of waveguides is deposited directly within the groove using the optically transparent silicone elastomer OE6520. Since this silicone flows, it spreads to fill the cavity formed by the groove. A top layer of SE1700 silicone seals the structure, serving as optical cladding. The structure is then heat cured at 120°C for 90 min. The printed optical fibre is cut at 45 degrees angle by a custom-made cutting nozzle. A razor blade (Wilkinson) is bent at 45 degrees angle and attached to a normal printing nozzle. Next the nozzle is loaded to the printer. The printer then moves in a diagonal direction parallel to the 45 degrees angle until the blade touches the glass, thus cutting the printed structures at an already specified position. Excess material is then removed. A layer of the white reflector silicone MS2002 is then deposited directly on the freshly cut surface. Prior to each printing step, the structure is exposed to a brief oxygen plasma session to improve interlayer adhesion. Finally, the free end of the silica optical fibre is coupled directly into a blue light LED source (470 nm, M470F3, Thorlabs) with the assistance of ceramic ferrule with similar core dimensions. Light transition measurements were conducted by inserting the free end of the printed optical fibre into the opening of the integrating chamber of an optical power meter (PM100D, S124C, Thorlabs). For the Tyndall effect experiments, the fibres were immersed into a solution of water-diluted colloidal milk particles.

Electrical fibres

Similar groove-shaped scaffolds are developed; however, here the groove is filled with the conductive Pt-based ink by ink-jetting or pipetting. This is followed by heating at 120°C for 5 min to remove the dispersing solvent. The beginning of the groove is covered with conductive epoxy (EPO-TEK H27D, Epoxy Technology) to which conventional electrical wires are attached. The free end of the electrical wires is used as a connection input to the device. A final layer of Sylgard 184 forms the electrical passivation. The conductive composite formed between Sylgard 184 and the platinum particles has resistivity of (9.8 ± 1.5) $\times 10^{-5} \Omega\text{m}$ (mean \pm StDev, $n = 4$).

Impedance spectra of individual electrodes (comprising of the active site, the electrically passivated interconnect and connector wire) were recorded with a potentiostat equipped with a frequency response analyser (AUTOLAB PGSTAT204, Metrohm). Frequencies in the range of $10\text{--}10^5 \text{ Hz}$ were scanned at the open circuit potential with an excitation amplitude of $10 \text{ mV}_{\text{RMS}}$. Measurements are performed with a Ag/AgCl reference electrode and a platinum coil counter electrode, which were immersed in the culture chamber of finished devices. For impedance measurements, the culture chamber was filled with phosphate-buffered saline (PBS).

Fluidic fibres

Here we take advantage of the high yield stress of the SE1700 silicone, which allows reproducible printing of overhanging and high aspect ratio features. As with the other components, a bottom layer is first created. Next, two additional Π -shaped lines are deposited, with a negative offset ($50 \mu\text{m}$) along the width of the structure. The resulting structure is pyramidal in shape and contains a hollow core. The core has circular cross-section with diameter $D = 135 \mu\text{m}$. The final structure is then thermally polymerized (120°C for 45 min). Connection to a fluid repository is ensured by the attachment of silicone tubings ($\varnothing 200 \mu\text{m}$) between the free end of the printed fluidic fibre and a syringe acting as the fluid reservoir. In a similar manner, curved lines as well as T- and Y-shaped bifurcations are developed. Flow rate experiments were performed with an eight-channel compact microfluidic controller (MFCS™-EX, Fluigent). In addition, injection of two food dye solutions of different colours (red and blue), at one end of a fluidic fibre at a flow rate of 0.1 mL min^{-1} , demonstrated the ability to support laminar flow. Water droplet formation experiments were conducted with the help of a low pressure syringe pump (neMESYS Low

Pressure module V2, CETONI GmbH). Transparent mineral oil (Sigma-Aldrich) and a solution of red food dye were injected from separate inputs (0.2 mL min^{-1}) at a T-junction fluidic fibre, and water in oil emulsions were acquired at the output of the fibre.

Integrated membrane

Here an array consisting of four freeform electrical fibres, one optical and one fluidic fibre is fabricated. In addition, the silicone elastomer Sylgard 184 is deposited over the array as an encapsulation medium. The structure is heat cured at 80°C for 45 min. In addition, a small amount of the silicone elastomer 734 Clear (Dow Corning) is deposited manually to ensure a more secure encapsulation around the device connectors. The structure is detached (peeled off) from the substrate and rotated along the length by 180° (flipped) providing access to the active sites of the functional fibres. Finally, a small circular-shaped cell chamber ($\varnothing 12 \text{ mm}$) is printed directly on the surface of the device, surrounding the cluster of active sites.

Scanning electron microscopy

Electron microscopy was performed on a JEOL JSM-7500F field emission scanning electron microscope. Prior to imaging, a thin layer of platinum was sputtered on the sample under investigation.

hiPSC culture

A human fibroblast-derived induced pluripotent stem cell line (CRTD5) was obtained from the iPS facility of the Center for Regenerative Therapies Dresden (CRTD)³⁰. Cells were propagated and maintained in mTESR™1 stem cell medium (Stem Cell Technologies, #85850) on Matrigel™-coated plates (Corning Life Sciences, #354234) under standard culturing conditions (37°C , 5% CO_2). hiPSCs were propagated using ReLeSR™ (Stem Cell Technologies, #05873) and routinely checked for mycoplasma contamination using the LookOut® Mycoplasma PCR Detection Kit (Sigma Aldrich, #D9307). The Cre-inducible Channelrhodopsin-2-EYFP expression cassette (Supplementary Fig. 3a) was genetically integrated by the PiggyBac transposon system into CRTD5 hiPSCs. The 4D-Nucleofector™ System (Lonza) was used to electroporate PiggyBac and transposase vectors into CRTD5 cells in suspension (X-Unit, P3 Primary Cell 4D-Nucleofector® X Kit L, program CB-156) following the manufacturer's guidelines. Briefly, $10 \mu\text{g}$ transposon DNA and $2 \mu\text{g}$ transposase vector (System Biosciences) were applied in $<10 \mu\text{L}$ volume to 600,000 CRTD5 cells. After nucleofections, cells were kept under constant ($20 \mu\text{g mL}^{-1}$) blasticidin (Thermo Fisher Scientific, #A1113903) selection.

hiPSC cardiomyocyte differentiation

hiPSCs were differentiated as a monolayer in 12-well plates when they reached $\sim 95\%$ confluence. Differentiation was initiated by a 48-h treatment with GSK3 β inhibitor CHIR99021 ($4 \mu\text{M}$ Sigma, #SML1046), followed by Wnt pathway inhibition mediated by IWP-2 ($5 \mu\text{M}$, Tocris, #3533) on days 2–4. During differentiation, cells were cultured in RPMI medium (Life Technologies, #72400047) supplemented with $500 \mu\text{g mL}^{-1}$ recombinant human albumin (Sigma, #A9731) and $213 \mu\text{g mL}^{-1}$ L-ascorbic acid 2-phosphate (Sigma, #A8960), referred to as medium CDM3, for 10 days³⁴. Spontaneous beating of hiPSC cardiomyocytes is observed around day 8. Selection was performed from day 10 to day 15 after starting the differentiation to increase cardiomyocyte purity in RPMI medium without glucose (Life Technologies, Cat# 11879), supplemented with 5 mM sodium dl-lactate (Sigma, #L4263), based on the protocol established by Burridge et al.³⁴.

Cre administration

On day 15 of differentiation, TAT-Cre protein (Merck Millipore, #SCR508, Lot# 2752483) was diluted to $0.59 \mu\text{M}$ in cell culture supernatant and added to the cells for 24 h at 37°C , 5% CO_2 . Fresh culture media was then added and cells were checked for transgene expression 3 days post induction using live fluorescence imaging. Optogenetic expression was further confirmed in fixed cultures stained for the EYFP that was fused to Channelrhodopsin-2.

Immunostainings

Cells were fixed with 4% formaldehyde solution in PBS for 15 min and stained overnight at 4°C for cardiac troponin-T (1:250, Thermo Fisher

number of samples is, at all times, indicated within the main text or in figure legends.

DATA AVAILABILITY

The data that support the findings of this study are available from the corresponding author I.R.M. upon reasonable request.

Received: 19 December 2019; Accepted: 29 May 2020;

Published online: 16 July 2020

Cytocompatibility test

For the cytocompatibility test, silicone chips of all different silicones and the silicon–platinum composite are prepared. Before cell seeding, the prepared silicone chips are cleaned and sterilized using 70% ethanol and ultraviolet irradiation. The sterile silicone chips are treated with air plasma to create a hydrophilic surface and allow for peptide binding. Directly afterwards, functionalization was performed using vitronectin as adhesive peptide. Therefore, samples are treated with a solution of $10 \mu\text{g mL}^{-1}$ Vitronectin XF™ in Cell Adhere™ dilution buffer (Stem Cell Technologies) for 2 h at room temperature and overnight at 4 °C. As negative control, samples are plasma treated and incubated in PBS for the same time. Directly before seeding, the silicone chips are briefly washed in PBS. The cells are cultivated for 3 days on the silicone materials. After this time, cells are fixed with 4% paraformaldehyde for 20 min. The fixed cells are stained with phalloidin555 (Abcam) for actin and DAPI (ThermoFisher) for cell nuclei. To determine cell density, cell nuclei are counted. For cell-covered area, the actin-covered area is quantified. Quantifications are performed using the threshold tool and the *analyse particles* plugin (Fiji/ImageJ).

Recording and stimulation tests

After generation and selection of hiPSC-derived cardiomyocytes, these cells were re-plated inside vitronectin-treated microphysiological platforms at a density of $250 \text{ cells mm}^{-2}$. Electrical recording is performed using an INTAN RHD2132 amplifier coupled with a computer via the RHD2000 USB interface board. The recording is done simultaneously from all four electrodes of the chip. The amplifier hardware bandwidth is set to 0.1–7500 Hz. The sampling rate is 5 kS s^{-1} . All recording and stimulation experiments were conducted inside a cell culture incubator at standard conditions of $37^\circ\text{C}/5\% \text{CO}_2/100\% \text{humidity}$.

For microfluidic infusion, isoproterenol diluted in culture medium at $10 \mu\text{M}$ and preheated to 37°C is injected manually at a rate of approximately $180 \mu\text{L min}^{-1}$. The final concentration of the drug in the cell culture chamber is around $2 \mu\text{M}$.

For optical stimulation, a blue light (470 nm) LED source (Thorlabs M470F3) is triggered by electrical pulses generated by an oscilloscope/function generator (Pico 2205A, Pico Technology). Pulse duration is set as 5% of the interpulse period and varies between 17 and 100 ms. The trigger pulses are also recorded with a RHD2000 USB interface board to synchronize the optical stimulation with electrical recordings.

For comparison, we made recordings with a commercial MEA. For MEA recordings, hiPSC cardiomyocytes were re-seeded after differentiation onto 59 recording electrodes MEAs (Multi Channel Systems, 60PdotMEA200/30iR-Au-gr) coated with fibronectin (Sigma Aldrich F4759, $10 \mu\text{g mL}^{-1}$). An MEA1060-Inv-BC system (Multi Channel Systems) with the heating plate set to 37°C was used for MEA recordings. MEAs were kept outside the incubator for no longer than 15 min. Raw electrode data were acquired via the MC_Rack software (Multi Channel Systems).

Imaging of printed structures

A ZEISS Axio Observer.A1 microscope equipped with a Mikrotron EoSens CL 1362 high-speed camera was used for capturing the water droplet formation. In addition, a ZEISS Axiovert 200M with Apotome microscope was used for capturing the cell micrographs. Other optical images were captured with a macro-lens. All sketches were designed with the help of the open source software Blender.

Statistics

In graphs and in the text, measurements are shown as averages from independent samples and errors represent one standard deviation. The

REFERENCES

1. Minev, I. R. et al. Electronic dura mater for long-term multimodal neural interfaces. *Science* **347**, 159–163 (2015).
2. Park, J. et al. Electromechanical cardioplasty using a wrapped elasto-conductive epicardial mesh. *Sci. Transl. Med.* **8**, 344ra386 (2016).
3. Feig, V. R., Tran, H., Lee, M. & Bao, Z. Mechanically tunable conductive interpenetrating network hydrogels that mimic the elastic moduli of biological tissue. *Nat. Commun.* **9**, 2740 (2018).
4. Tondera, C. et al. Highly conductive, stretchable, and cell-adhesive hydrogel by nanoclay doping. *Small* **15**, 1901406 (2019).
5. Liu, H. et al. Microdevice arrays with strain sensors for 3D mechanical stimulation and monitoring of engineered tissues. *Biomaterials* **172**, 30–40 (2018).
6. Yu, Z. et al. Monitoring hippocampus electrical activity in vitro on an elastically deformable microelectrode array. *J. Neurotrauma* **26**, 1135–1145 (2009).
7. Jonsson, A. et al. Bioelectronic neural pixel: chemical stimulation and electrical sensing at the same site. *Proc. Natl. Acad. Sci. USA* **113**, 9440–9445 (2016).
8. Welkenhuysen, M. et al. An integrated multi-electrode-optrode array for in vitro optogenetics. *Sci. Rep.* **6**, 20353 (2016).
9. Yamamoto, H. et al. Ultrasoft silicone gel as a biomimetic passivation layer in inkjet-printed 3D MEA devices. *Adv. Biosyst.* **3**, 1900130 (2019).
10. Besser, R. R. et al. Engineered microenvironments for maturation of stem cell derived cardiac myocytes. *Theranostics* **8**, 124–140 (2018).
11. Kroll, K. et al. Electro-mechanical conditioning of human iPSC-derived cardiomyocytes for translational research. *Prog. Biophys. Mol. Biol.* **130**, 212–222 (2017).
12. Oleaga, C. et al. A human in vitro platform for the evaluation of pharmacology strategies in cardiac ischemia. *APL Bioeng.* **3**, 036103 (2019).
13. Lind, J. U. et al. Instrumented cardiac microphysiological devices via multimaterial three-dimensional printing. *Nat. Mater.* **16**, 303–308 (2017).
14. Young, A. T., Rivera, K. R., Erb, P. D. & Daniele, M. A. Monitoring of microphysiological systems: integrating sensors and real-time data analysis toward autonomous decision-making. *ACS Sens.* **4**, 1454–1464 (2019).
15. Frank, J. A., Antonini, M.-J. & Anikeeva, P. Next-generation interfaces for studying neural function. *Nat. Biotechnol.* **37**, 1013–1023 (2019).
16. Vachicouras, N. et al. Microstructured thin-film electrode technology enables proof of concept of scalable, soft auditory brainstem implants. *Sci. Transl. Med.* **11**, eaax9487 (2019).
17. Yang, X. et al. Bioinspired neuron-like electronics. *Nat. Mater.* **18**, 510–517 (2019).
18. Chung, H. U. et al. Binodal, wireless epidermal electronic systems with in-sensor analytics for neonatal intensive care. *Science* **363**, eaau0780 (2019).
19. Roche, E. T. et al. Soft robotic sleeve supports heart function. *Sci. Transl. Med.* **9**, eaaf3925 (2017).
20. Park, S.-J. et al. Phototactic guidance of a tissue-engineered soft-robotic ray. *Science* **353**, 158 (2016).
21. Miyashita, S. et al. Ingestible, controllable, and degradable origami robot for patching stomach wounds. In *2016 IEEE International Conference on Robotics and Automation (ICRA)*. 909–916 (IEEE, 2016).
22. Kim, Y., Parada, G. A., Liu, S. & Zhao, X. Ferromagnetic soft continuum robots. *Sci. Robot.* **4**, eaax7329 (2019).
23. Valentine, A. D. et al. Hybrid 3D printing of soft electronics. *Adv. Mater.* **29**, 1703817 (2017).
24. Athanasiadis, M., Pak, A., Afanasyenka, D. & Minev, I. R. Direct writing of elastic fibers with optical, electrical, and microfluidic functionality. *Adv. Mater. Technol.* **4**, 1800659 (2019).
25. Truby, R. L. et al. Soft somatosensitive actuators via embedded 3D printing. *Adv. Mater.* **30**, 1706383 (2018).
26. Zhijie, Z. et al. 3D printed functional and biological materials on moving freeform surfaces. *Adv. Mater.* **30**, 1707495 (2018).
27. Lee, S. et al. Ultrasoft electronics to monitor dynamically pulsing cardiomyocytes. *Nat. Nanotechnol.* **14**, 156–160 (2019).
28. Kolesky, D. B. et al. 3D bioprinting of vascularized, heterogeneous cell-laden tissue constructs. *Adv. Mater.* **26**, 3124–3130 (2014).

29. Klapper, S. D. et al. On-demand optogenetic activation of human stem-cell-derived neurons. *Sci. Rep.* **7**, 14450 (2017).
30. Kutsche, L. K. et al. Combined experimental and system-level analyses reveal the complex regulatory network of miR-124 during human neurogenesis. *Cell Syst.* **7**, 438.e8–452.e8 (2018).
31. Minev, I. R., Wenger, N., Courtine, G. & Lacour, S. P. Research update: platinum-elastomer mesocomposite as neural electrode coating. *APL Mater.* **3**, 014701 (2015).
32. Franks, W., Schenker, I., Schmutz, P. & Hierlemann, A. Impedance characterization and modeling of electrodes for biomedical applications. *IEEE Trans. Biomed. Eng.* **52**, 1295–1302 (2005).
33. Oh, K. W., Lee, K., Ahn, B. & Furlani, E. P. Design of pressure-driven microfluidic networks using electric circuit analogy. *Lab Chip* **12**, 515–545 (2012).
34. Burridge, P. W. et al. Chemically defined generation of human cardiomyocytes. *Nat. Methods* **11**, 855 (2014).
35. Lian, X. et al. Robust cardiomyocyte differentiation from human pluripotent stem cells via temporal modulation of canonical Wnt signaling. *Proc. Natl Acad. Sci. USA* **109**, E1848–E1857 (2012).
36. Gordan, R., Gwathmey, J. K. & Xie, L.-H. Autonomic and endocrine control of cardiovascular function. *World J. Cardiol.* **7**, 204–214 (2015).
37. Rehnel, S. et al. Frequency-dependent multi-well cardiotoxicity screening enabled by optogenetic stimulation. *Int. J. Mol. Sci.* **18**, 2634 (2017).
38. Boycott, H. E. et al. Shear stress triggers insertion of voltage-gated potassium channels from intracellular compartments in atrial myocytes. *Proc. Natl Acad. Sci. USA* **110**, E3955–E3964 (2013).
39. Xu, L. et al. 3D multifunctional integumentary membranes for spatiotemporal cardiac measurements and stimulation across the entire epicardium. *Nat. Commun.* **5**, 3329 (2014).
40. Drack, M. et al. An imperceptible plastic electronic wrap. *Adv. Mater.* **27**, 34–40 (2015).
41. Raney, J. R. & Lewis, J. A. Printing mesoscale architectures. *MRS Bull.* **40**, 943–950 (2015).
42. Pavesi, A. et al. Controlled electromechanical cell stimulation on-a-chip. *Sci. Rep.* **5**, 11800 (2015).
43. Egusa, H. et al. Application of cyclic strain for accelerated skeletal myogenic differentiation of mouse bone marrow-derived mesenchymal stromal cells with cell alignment. *Tissue Eng. Part A* **19**, 770–782 (2012).
44. McCain, M. L., Sheehy, S. P., Grosberg, A., Goss, J. A. & Parker, K. K. Recapitulating maladaptive, multiscale remodeling of failing myocardium on a chip. *Proc. Natl Acad. Sci. USA* **110**, 9770–9775 (2013).

ACKNOWLEDGEMENTS

We thank the Light Microscopy and iPSC core facilities of BIOTEC/CRTD for their help with imaging and stem cell protocols, Simon Klapper and Anka Kempe for help with electroporation of vectors into CRTD5 line and methodological advice. We acknowledge funding from Volkswagen Foundation (Freigeist 91 690), ERC starting grant

(804005-IntegraBrain) and Center for Advancing Electronics Dresden (cfaed). V.B. was supported by the Volkswagen Foundation (Freigeist A110720) and by an ERC starting grant (678071-ProNeurons). O.B. was supported by the Center for Regenerative Therapies Dresden, the Karolinska Institutet, the Swedish Research Council, the Ragnar Söderberg Foundation, and the Åke Wiberg Foundation.

AUTHOR CONTRIBUTIONS

M.A., D.A., W.D., C.T. and F.M. performed the experiments. All authors contributed to data analysis, manuscript writing and project coordination.

COMPETING INTERESTS

The authors declare no competing interests.

ADDITIONAL INFORMATION

Supplementary information is available for this paper at <https://doi.org/10.1038/s41528-020-0075-z>.

Correspondence and requests for materials should be addressed to I.R.M.

Reprints and permission information is available at <http://www.nature.com/reprints>

Publisher's note Springer Nature remains neutral with regard to jurisdictional claims in published maps and institutional affiliations.



Open Access This article is licensed under a Creative Commons Attribution 4.0 International License, which permits use, sharing, adaptation, distribution and reproduction in any medium or format, as long as you give appropriate credit to the original author(s) and the source, provide a link to the Creative Commons license, and indicate if changes were made. The images or other third party material in this article are included in the article's Creative Commons license, unless indicated otherwise in a credit line to the material. If material is not included in the article's Creative Commons license and your intended use is not permitted by statutory regulation or exceeds the permitted use, you will need to obtain permission directly from the copyright holder. To view a copy of this license, visit <http://creativecommons.org/licenses/by/4.0/>.

© The Author(s) 2020